J Mater Sci: Mater Electron (2022) 33:18054–18071

Structural and optical properties of barium titanium borate glasses doped with ytterbium

S. Y. Marzouk[1], M. A. Azooz[2], H. M. Elsaghier[3,*], Nehad A. Zidan[3], and W. Abbas[1]

[1] *Basic and Applied Science Department, College of Engineering and Technology, Arab Academy for Science, Technology, and Maritime Transport, Cairo, Egypt*
[2] *Glass Research Department, National Research Centre, Dokki, Giza, Egypt*
[3] *Engineering Physics and Mathematics Department, Faculty of Engineering (Mataria), Helwan University, Cairo, Egypt*

Received: 28 April 2022
Accepted: 25 June 2022
Published online: 21 July 2022

ABSTRACT

Barium titanium borate glasses doped with ytterbium ions were fabricated via standard melt quenching technique. The building structure of the glass matrices doped with ascendant ratios of ytterbium ions were studied using Raman and FTIR spectroscopies. The UV–Vis–NIR optical absorption spectra were investigated and used to calculate optical bandgaps, Urbach energies, refractive indices, metallization criterion, optical basicity, and dispersion parameters. The absorption and emission cross-sections and gain spectra for $^2F_{5/2} \rightarrow {}^2F_{7/2}$ transition of ytterbium ions were investigated. The high values of the emission cross-sections of the studied glasses make them strong candidates for laser and amplifier applications.

1 Introduction

Alkali/alkaline earth borate glasses doped with transition metal elements, rare earth elements or both attracted the interest of researchers due to the importance of these glasses in developing many technological applications such as solid-state lasers, solar energy converters, optical fibers, and electronic devices [1–3]. Barium borate glasses have acquired great importance due to their unique optical properties, low melting point, high thermal and mechanical stability, and good solubility of rare earth ions as well as transition metals [4–6]. The fundamental structural units of borate-based glasses are trigonal BO_3 and tetrahedral BO_4 which can combine to form different structural groups such as diborates, tetraborates, orthoborates, pentaborates, metaborates, and boroxol rings. The coordination number of the boron atom can be easily changed from three to four or vice versa depending on the type and the concentration of the added modifier [7–10].

The introduction of transition metals into glasses improves the structural, optical, electrical, and magnetic properties of them due to the multiplicity of valance states of these elements, which depend mainly on the glass composition and melting conditions [8, 11, 12]. Among transition metal oxides, TiO_2 is a useful glass constituent for preparation some

Address correspondence to E-mail: Hossam_Elsaghier@m-eng.helwan.edu.eg; Hossam_Elsaghier@yahoo.com

https://doi.org/10.1007/s10854-022-08665-0

special optical glasses and glass-ceramics. Titanium ions usually exist in the glassy host in trivalent and tetravalent valence states and participate in the glassy matrix with TiO_4, TiO_6, and sometimes TiO_5 structural groups [13].

Barium titanate-based glasses are promising materials due to their unique and distinctive structural, optical, and electrical properties which make them good candidates in many modern applications such as sensors and transducers, electronics, bioactive materials, non-linear optical devices, and reversible electrodes [14, 15]. The incorporation of barium titanate with any glass former helps to form a homogeneous glass matrix and enhances the radiation shielding properties of this matrix [16]. Glasses containing rare earth elements as luminescent centers are considered as an important class of photonic materials due to their unique and distinct spectroscopic properties resulting from f–f transitions in the visible and near to mid IR spectral ranges [17, 18]. The luminescent properties of these glasses are mainly dependent on the glass type, composition, and the ratio of the rare earth elements [19].

The objective of this work is to investigate the impact of Yb^{3+} ions on the structural and optical properties of barium titanium borate glasses as optical materials.

2 Experimental details

2.1 Glass fabrication

Pure chemicals of boric acid (H_3BO_3), titanium dioxide (TiO_2), barium carbonate ($BaCO_3$), and ytterbium oxide (Yb_2O_3) were used as starting materials to synthesize Yb^{3+}-doped barium titanium borate glasses by the standard melting-quenching method. Appropriate molar ratios of the starting materials were weighed, thoroughly mixed, and melted in a porcelain crucible using an electric furnace (VECSTAR, UK) at 1100 ± 10 °C for 2 h. The molten materials were rotated and checked every half hour to obtain a high degree of homogeneity, then casted into slightly warm stainless-steel molds and rapidly moved to a muffle furnace for annealing at 330 ± 5 °C for half hour. The molar composition of the synthesized glasses and their codes are presented in Table 1.

2.2 Density and molar volume measurements

Archimedes method was utilized for measuring the density (ρ) of the bulk glasses by weighing them in both of air and xylene (0.86 g/cm^3) based on the next relation:

$$\rho = \frac{W_a \times \rho_x}{W_a - W_x} \frac{g}{cm^3}, \quad (1)$$

where W_a is the glass weight in air, W_x is the glass weight in xylene, and ρ_x is the xylene density. The molar volume (V_m) of the glasses is estimated using the relation $V_m = Mwt/\rho$, where Mwt is the glass molecular weight.

2.3 Spectroscopic measurements

Raman spectra were recorded in the wavenumber range 40–3750 cm^{-1} using SENTERRA Raman microscope (Bruker, Germany) with a laser excitation wavelength of 785 nm and power of 50 mW. The FTIR absorption spectra were recorded using computerized FTIR spectrometer (Bruker, Vertex 70v, Germany) covers the wavenumber range 4000–400 cm^{-1}. The UV–vis–NIR absorption spectra were recorded using a single monochromatic spectrophotometer (JASCO, V-770, Japan) covers the wavelength range 2500–190 nm. XRD spectra were recorded using a diffractometer (Philips, PW-1390) in 2Θ range from 5° to 70°.

3 Results and discussion

3.1 XRD spectra

Figure 1 shows the XRD spectra of the studied glasses in the range of 5°–70°. The non-presence of a sharp peak in the XRD pattern confirms the

Table 1 Compositions of barium titanium borate glasses doped with Yb_2O_3 in mol% and their codes

Sample code	B_2O_3	TiO_2	BaO	Yb_2O_3
BTiBaYb0	54.250	8.320	37.430	0
BTiBaYb1	54.112	8.301	37.329	0.258
BTiBaYb3	53.835	8.259	37.138	0.769
BTiBaYb5	53.560	8.216	36.948	1.275

amorphous or non-crystalline phase of the synthesized glasses [20].

3.2 Density and molar volume

The dependance of the density (ρ) and molar volume (V_m) of the studied glasses on Yb_2O_3 content is shown in Fig. 2. The addition of Yb_2O_3 with ascending ratios increases the density of the glasses from 3.652 to 3.761 g/cm^3 due to the replacement of the lighter mass content B_2O_3, TiO_2, and BaO by the heavier mass content Yb_2O_3 [4]. Moreover, replacing the oxides of boron, titanium, and barium with ytterbium oxide increases the number of oxygen ions within the glass matrix, which promotes the conversion of triangular BO_3 units to tetrahedral BO_4 units, and because the density of BO_4 units is greater than that of BO_3 units, this conversion promotes an increase in the density of the glass [21, 22]. The molar volume is found to decrease from 27.875 to 27.784 cm^3/mol then increase to 28.06 cm^3/mol due to the difference between ionic radii of Yb (0.985 Å) and other cations (Ba 1.35 Å, Ti 0.74 Å, B 0.23 Å) within the glass matrix. Thus, both the rigidity and compactness of the glasses diminishes as a result of the creation of more non-bridging oxygens [21]. The obtained values of the density and molar volume are presented in Table 2.

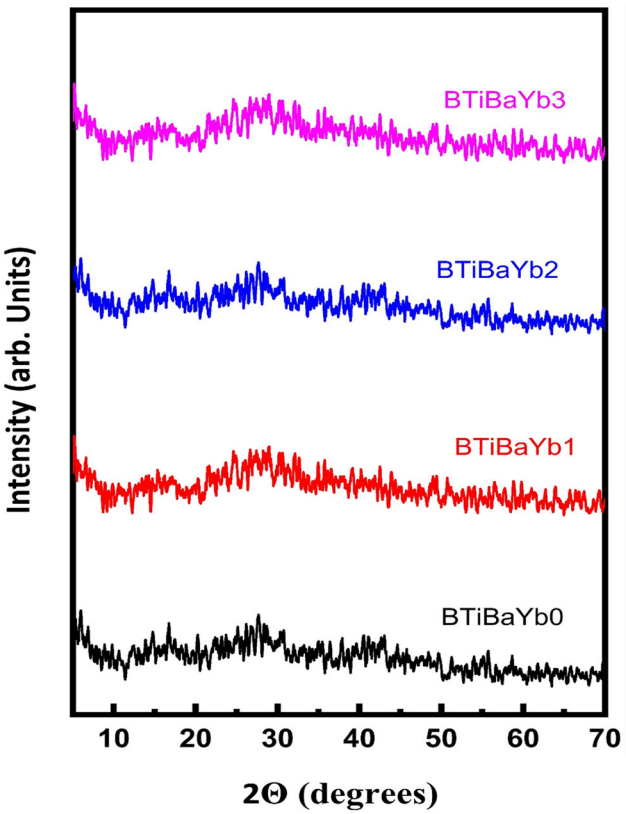

Fig. 1 XRD spectra of Yb^{3+}-doped barium titanium borate glasses

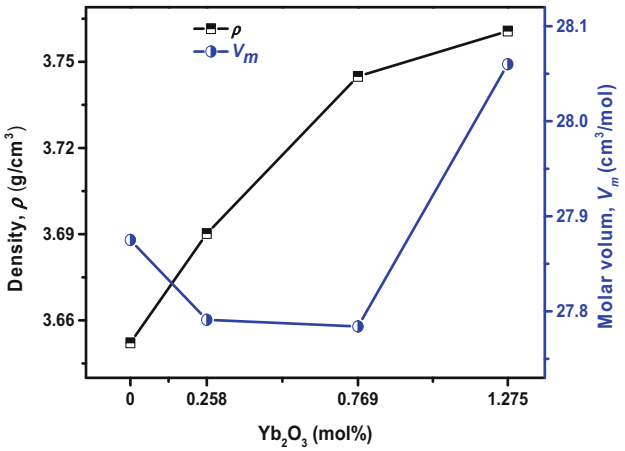

Fig. 2 Density and molar volume as a function of Yb_2O_3 content

The obtained values of the density and molar volume are utilized to calculate some physical parameters such as Yb^{3+} ions concentration (N), Yb^{3+} ions separation (R), oxygen packing density (OPD), and mean boron–boron separation ($<d_{B-B}>$) based on the next relationships [7, 23, 24]:

$$N = 2\left(\frac{\rho x_{Yb_2O_3}}{Mwt}\right)N_A \tag{2}$$

$$R = \sqrt[3]{\frac{1}{N}} \tag{3}$$

$$\mathrm{OPD} = \frac{z\rho}{Mwt} \times 1000 \tag{4}$$

$$<d_{B-B}> = \left(\frac{V_m}{2N_A(1 - x_{B_2O_3})}\right)^{1/3}, \tag{5}$$

where x_{Yb2O3} is the molar fraction of Yb_2O_3, N_A is Avogadro's number, z is the number of oxygen atoms in the glass composition, and x_{B2O3} is the molar fraction of B_2O_3. The N values increase as the concentration of Yb_2O_3 increases while the R values decrease. The OPD values increase until 0.769 mol% of Yb_2O_3 then decrease while the $<d_{B-B}>$ values have opposite trend for the same concentrations. The observed increase in the OPD and the observed decrease in the $<d_{B-B}>$ are the result of the compactness of the glass matrix with increasing the ratio of Yb_2O_3. The values of N, R, OPD, and $<d_{B-B}>$ are presented in Table 2.

Table 2 Density (ρ), molar volume (V_m), ytterbium ions concentration (N), mean ytterbium ions separation (R), oxygen packing density (OPD), and mean boron–boron separation ($<d_{B-B}>$) of Yb_2O_3-doped barium titanium borate glasses

Sample code	ρ (g/cm^3)	V_m (cm^3/mol)	$N \times 10^{20}$ (cm^{-3})	R (nm)	OPD (mol/L)	$<d_{B-B}>$ (Å)
BTiBaYb0	3.652	27.875	–	–	77.784	3.6984
BTiBaYb1	3.690	27.791	1.118	2.076	78.097	3.6910
BTiBaYb3	3.745	27.784	3.334	1.422	78.270	3.6833
BTiBaYb5	3.761	28.060	5.473	1.223	77.649	3.6881

3.3 Raman spectra

The Gaussian deconvolution of the Raman spectra for the studied glasses are shown in Fig. 3. The deconvoluted spectrum of the base undoped glass (BTiBaYb0) reveals eleven bands centered at 77 and 223 cm^{-1} due to vibrations of Ba^{2+} ions and Ti–O bonds, respectively [25, 26], 418 and 1140 cm^{-1} due to vibrations of diborate groups [27, 28], 540 and 901 cm^{-1} due to bending and stretching vibrations of orthoborate units, respectively [29, 30], 794 cm^{-1} due to vibration of planar six membered borate rings containing one BO_4 tetrahedron [31], 1007 cm^{-1} due to asymmetric stretching modes of tetrahedral borate units [5], 1281 cm^{-1} due to vibration of pyroborate groups [31], 1413 cm^{-1} due to vibration of non-bridging oxygens from various B–O structural units [32], and 1488 cm^{-1} due to vibration of BO_2O^- triangles connected with other borate triangular units [30]. The addition of Yb_2O_3 into host glass matrix with different ratios leads to the following modifications: (i) The formation of new bands in the range 707–736 cm^{-1} and 1502–1666 cm^{-1} due to the vibrations of B–O bonds in BO_4 units and metaborate rings, respectively [28, 29, 33–35]. (ii) The absence of the band at 1281 cm^{-1} in the BTiBaYb1 and BTiBaYb3 glasses shows the non-presence of pyroborate groups in these glasses [31].

Sekhar et al. [36] studied the deconvoluted Raman spectra of the $Na_2B_4O_7$–CdO–CuO–$BaTiO_3$ glasses which revealed distinctive bands at 733–768 cm^{-1} due to the vibrations of B–O–B linkages in the six membered borate rings with BO_4 tetrahedral, 842–877 cm^{-1} due to the vibration of orthoborate units and 1180–1375 cm^{-1} due to the stretching vibration of B–O$^-$ with non-bridging oxygens. The present work is in line with the results reported by Sekhar et al.

3.4 FTIR absorption spectra

The FTIR spectra of the studied glasses are shown in Fig. 4. The spectrum of the base undoped glass (BTiBaYb0) reveals a small band in the region 458–501 cm^{-1} with two peaks at 469 and 483 cm^{-1} due to vibration of barium ions [37]. Furthermore, a broad band in the region 545–760 cm^{-1} with its peak at 625 cm^{-1} is ascribed to vibration of titanium–oxygen bond in TiO_6 groups [38]. Moreover, a broad band in the region 776–1167 cm^{-1} is attributed to stretching vibration of BO_4 groups [39]. In addition, a broad band in the region 1195–1569 cm^{-1} with its center at 1384 cm^{-1} is attributed to stretching vibration of boron–oxygen bond in BO_3 groups [40]. A medium band in the region 1573–1728 cm^{-1} with two peaks at 1618 and 1638 cm^{-1} is ascribed to vibration of water and OH groups [39, 41]. The incorporation of Yb_2O_3 into glass matrix with different ratios leads to the following modifications: (i) The intensity of the first band (458–501 cm^{-1}) decreases with increasing the concentration of Yb^{3+} ions. (ii) The second band (545–760 cm^{-1}) becomes more broadened and splits into two bands centred at 572 and 721 cm^{-1} due to the bending modes of various borate groups and the vibrations of TiO_4 groups, respectively [38, 41]. (iii) The intensity of the third band (776–1167 cm^{-1}) increases with increasing the concentration of Yb^{3+} ions. (iv) The fourth band (1195–1569 cm^{-1}) becomes more broadened and splits into two bands with their peaks at 1207 and 1384 cm^{-1} due to the stretching vibrations of BO_4 and BO_3 groups, respectively, in the BTiBaYb1 and BTiBaYb5 glasses [39, 40]. (v) The intensity of the fifth band (1573–1728 cm^{-1}) decreases with increasing the concentration of Yb^{3+} ions. The obtained analysis from FTIR spectra are consistent and in agreement with that of Raman spectra.

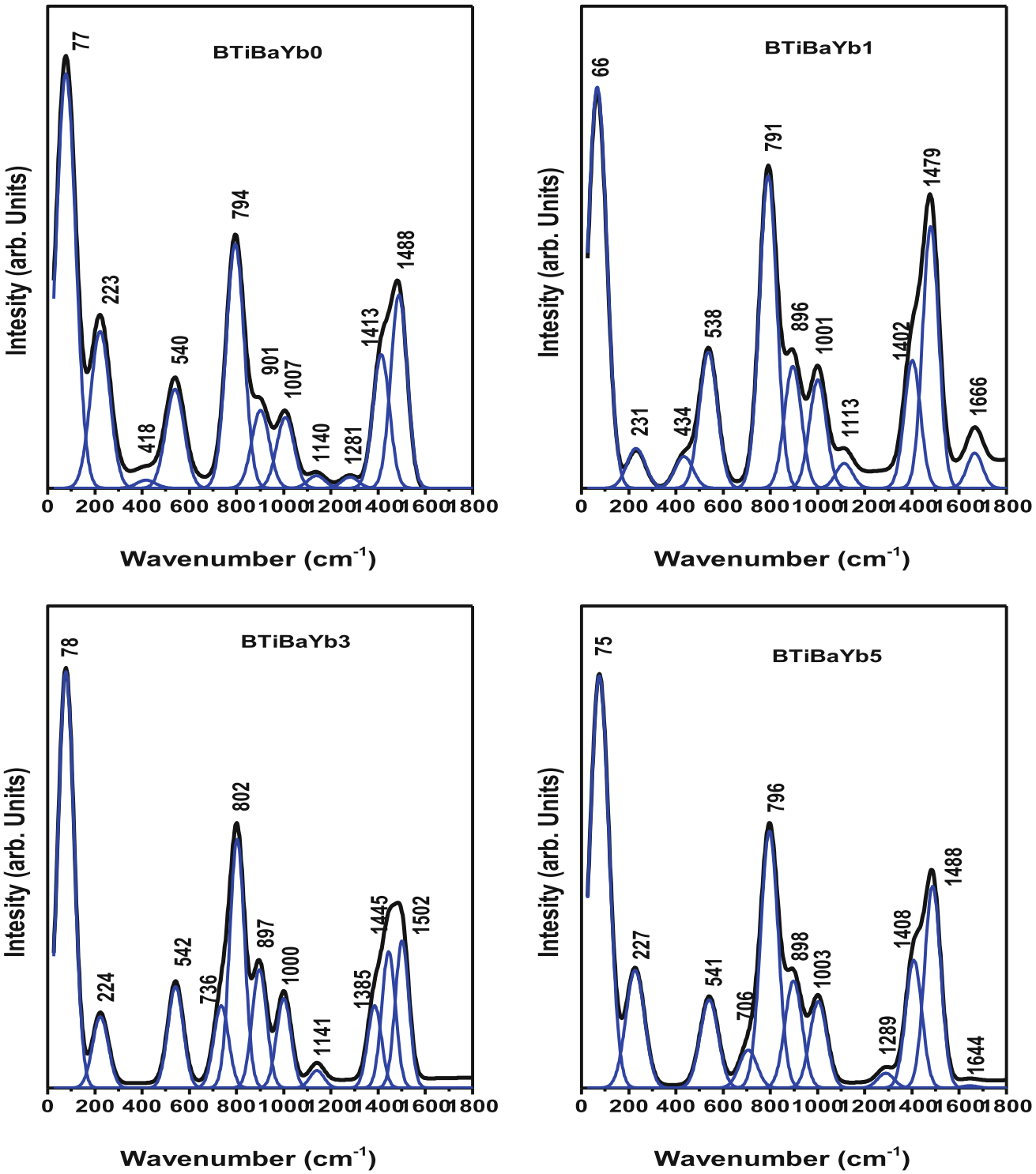

Fig. 3 Deconvoluted Raman spectra of Yb^{3+}-doped barium titanium borate glasses

3.5 Optical absorption spectra

The optical absorption spectra of the studied glasses are displayed in Fig. 5. The base undoped glass (BTiBaYb0) exhibits an absorption band in the UV region due to the existence of inevitable iron impurities within the raw materials [42]. The addition of Yb_2O_3 with different ratios leads to the formation of distinctive broad absorption band in the NIR region

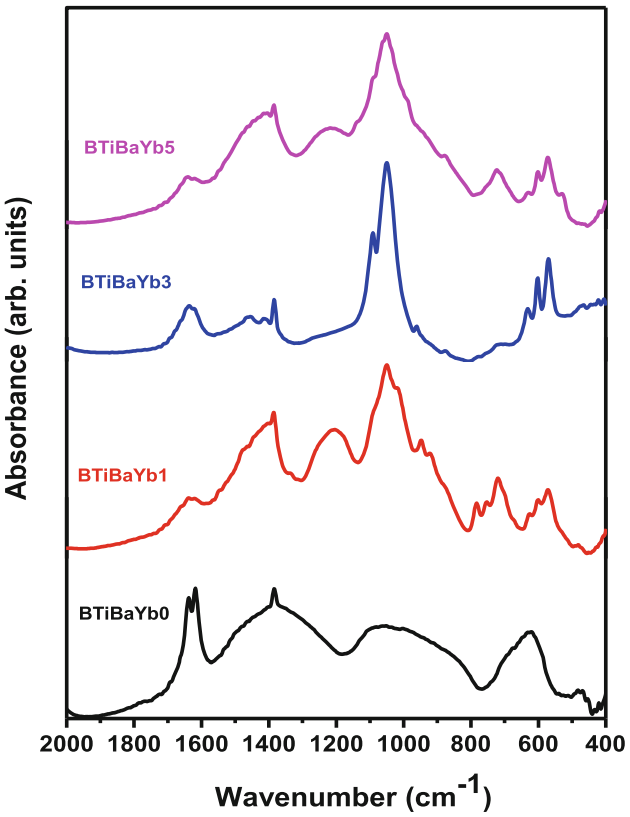

Fig. 4 FTIR absorption spectra of Yb^{3+}-doped barium titanium borate glasses

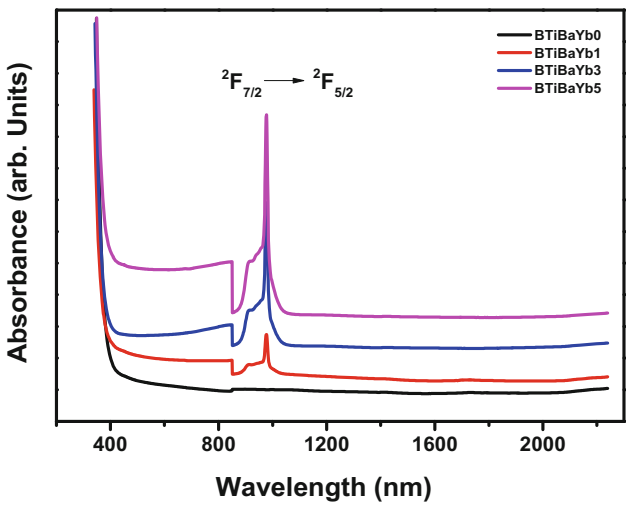

Fig. 5 UV–vis–NIR absorption spectra of Yb^{3+}-doped barium titanium borate glasses

at 977 nm due to the electronic transition from the $^2F_{7/2}$ ground state to the $^2F_{5/2}$ higher excited state [43]. The intensity of this band increases as the ratio of Yb_2O_3 increases.

3.6 Optical bandgap and Urbach energy

Moot and Davis theory is utilized to calculate the optical bandgap energy (E_g) from the optical absorption edge. The absorption coefficient (α) relevant to the absorption edge is determined using the relationship $\alpha = 2.303\ A/d$, where A is the optical absorption and d is the glass thickness. The relationship between α and E_g is given by [44]:

$$\alpha h\upsilon = B(h\upsilon - E_g)^r, \tag{6}$$

where $h\upsilon$ is the incident photon energy, B is constant, and r is the electronic transition index which holds the value of 2 for indirect allowed transition. Figure 6 shows Tauc's plots, i.e., $(\alpha h\upsilon)^{1/2}$ versus $h\upsilon$ for all glasses. The values of E_g are determined by extrapolating the linear parts of the curves to intercept the $h\upsilon$-axis at zero absorption coefficient. The values of E_g are recorded in Table 3 and found to be 3.198, 3.168, 3.140, and 3.115 eV for BTiBaYb0, BTiBaYb1, BTiBaYb3, and BTiBaYb5 glasses, respectively. The observed decrease in the values of E_g is ascribed to the excess of the non-bridging oxygens inside the glass network with increasing the ratio of Yb_2O_3 [45, 46].

Also, the absorption spectrum fitting (ASF) method is utilized to calculate the optical bandgap energy (E_g^{ASF}). According to the ASF method, Eq. (6) can be written in terms of optical absorbance (A) and photon wavelength (λ) as follow [47, 48]:

$$A = D\lambda(\lambda^{-1} - \lambda_g^{-1})^r, \tag{7}$$

where $D = [Bd(hc)^{r-1}/2.303]$, d is the glass thickness, h is Planck's constant, c is the light speed, and λ_g is the photon wavelength corresponding to the E_g^{ASF}. Figure 7 shows the plots of $(A/\lambda)^{1/2}$ versus λ^{-1} for all glasses. The values of λ_g^{-1} are determined by extrapolating the linear parts of the curves to intercept the λ^{-1}-axis at zero absorbance. The values of E_g^{ASF} are calculated from Eq. (8) and recorded in Table 3.

$$E_g^{ASF} = 1239.83 \times \lambda_g^{-1} \tag{8}$$

The values of E_g^{ASF} are found to be 3.194, 3.170, 3.137, and 3.113 eV for BTiBaYb0, BTiBaYb1, BTiBaYb3, and BTiBaYb5 glasses, respectively. From Table 3, it can be seen the values of E_g and E_g^{ASF} are matched and in agreement with each other which enhances the formation of non-bridging oxygens. The

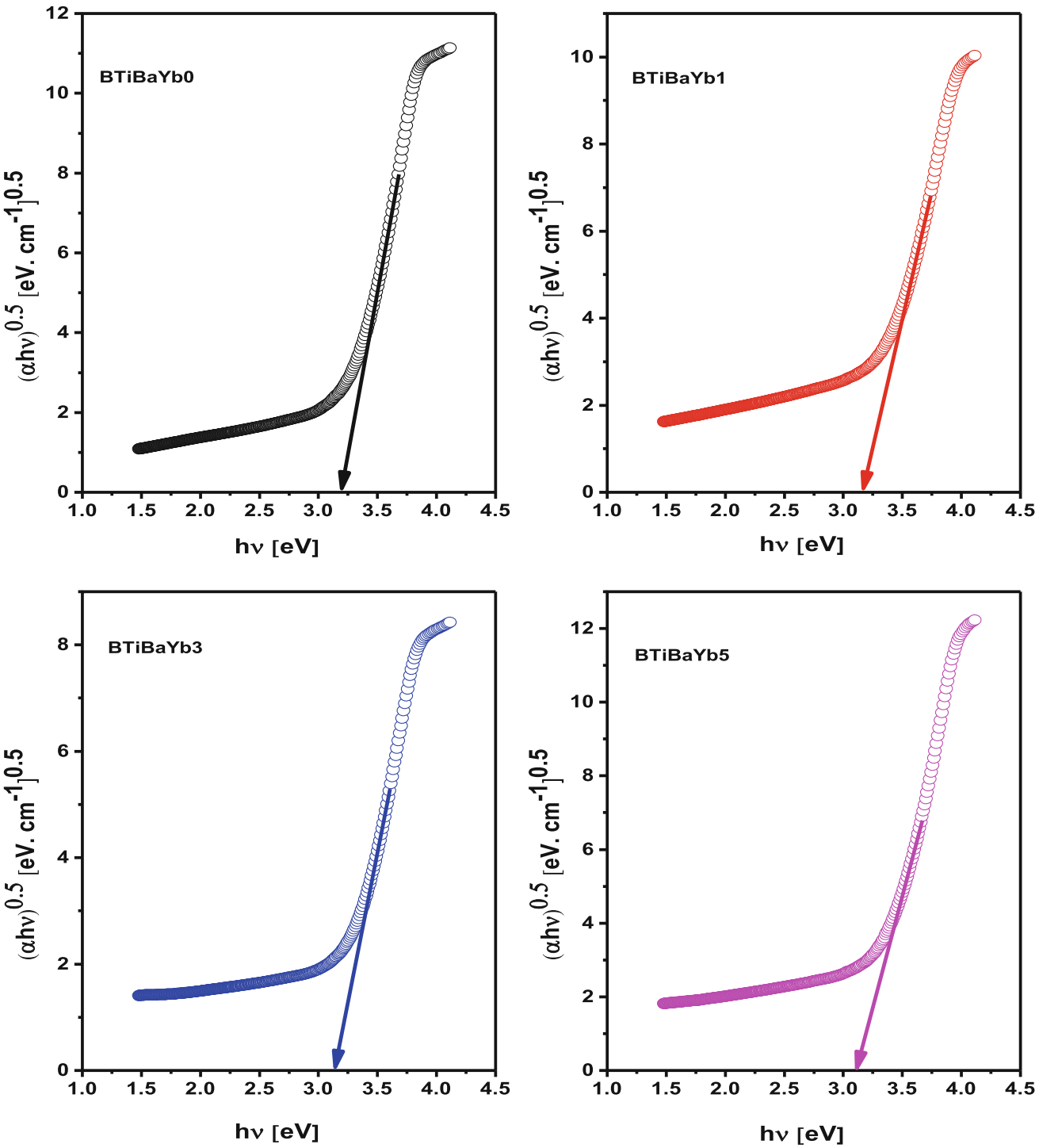

Fig. 6 $(\alpha h\upsilon)^{1/2}$ vs. $h\upsilon$ for Yb^{3+}-doped barium titanium borate glasses

average values of the optical bandgaps ($E_g^{avg} = E_g + E_g^{ASF}/2$) are calculated and recorded in Table 3.

Urbach energy (ΔE) is a measure of the disorders inside the glassy matrix and related to the logarithm of the absorption coefficient through the relationship [49]:

$$\mathrm{Ln}(\alpha) = \text{constant} + \frac{h\upsilon}{\Delta E} \tag{9}$$

Table 3 Optical bandgap (E_g & E_g^{ASF}), average optical bandgap (E_g^{avg}), Urbach energy (ΔE), and linear refractive index (n_{D-S}) of Yb_2O_3 doped barium titanium borate glasses

Sample code	E_g (eV) [Tauc's method]	E_g^{ASF} (eV) [ASF method]	E_g^{avg} (eV)	ΔE (eV)	n_{D-S}
BTiBaYb0	3.198	3.194	3.196	0.210	2.346
BTiBaYb1	3.168	3.170	3.169	0.279	2.353
BTiBaYb3	3.140	3.137	3.139	0.228	2.361
BTiBaYb5	3.115	3.113	3.114	0.255	2.367

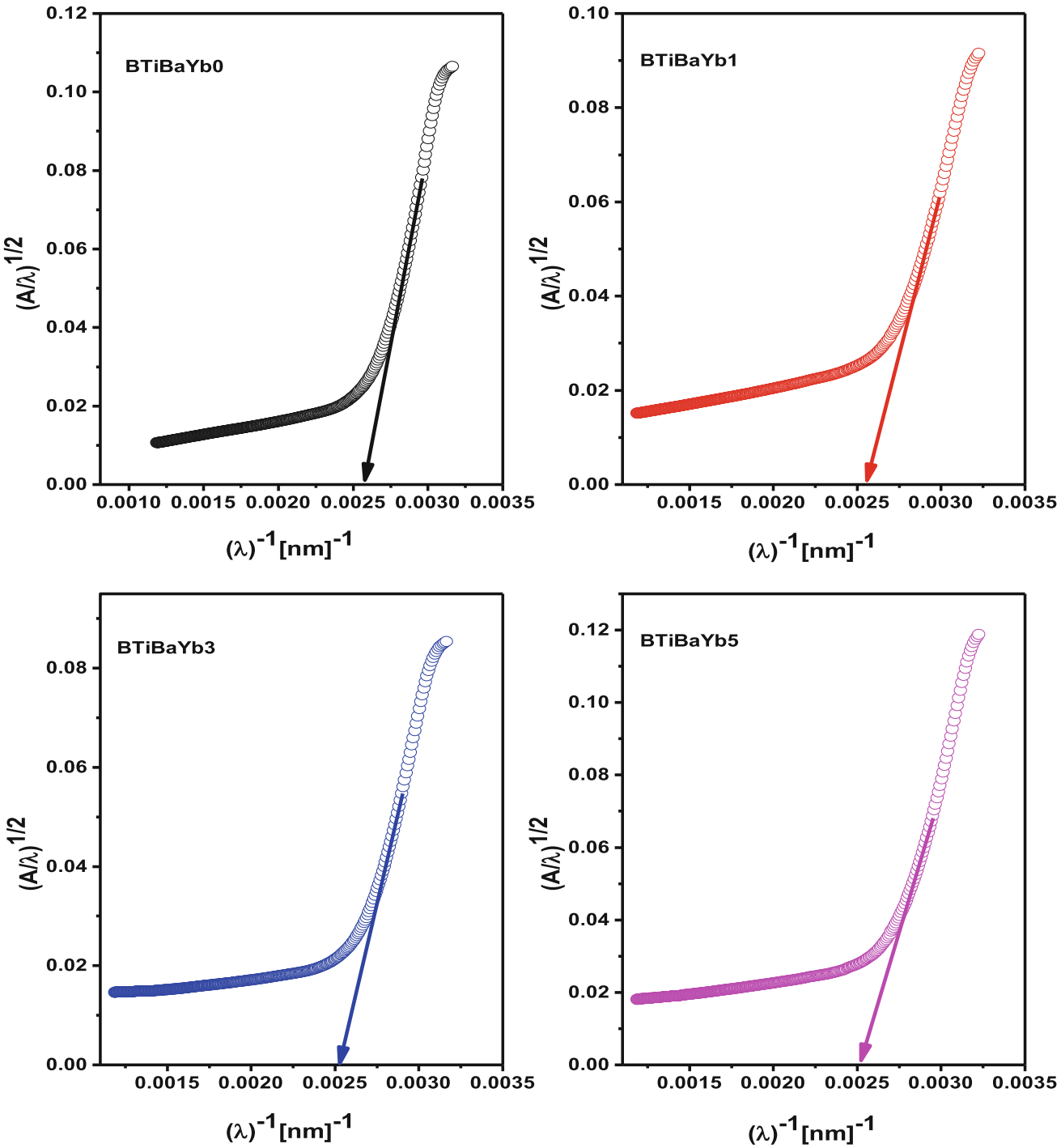

Fig. 7 $(A/\lambda)^{1/2}$ vs. (λ^{-1}) for Yb^{3+}-doped barium titanium borate glasses

The values of ΔE are calculated by obtaining the reciprocal of the slope of the linear parts of ln (α) versus $h\nu$ plots and are recorded in Table 3. The plots of ln (α) vs. $h\nu$ for all glasses are presented in Fig. 8. The values of ΔE are found to be 0.210, 0.279, 0.228, and 0.255 eV for for BTiBaYb0, BTiBaYb1, BTiBaYb3, and BTiBaYb5 glasses, respectively. The BTiBaYb1 glass has the highest value of ΔE, and thus the highest degree of disorders. The BTiBaYb0 glass has the lowest value of ΔE, and thus the lowest degree of disorders which means more homogeneity and stable structure with minimal defects [49, 50].

3.7 Refractive index and dispersion parameters

The average values of the optical bandgaps (E_g^{avg}) are employed to calculate the corresponding linear refractive indices (n_{D-S}) at high frequencies using Dimitrov–Sakka relationship [45]:

$$n_{D-S} = \left(6\sqrt{\frac{5}{E_g^{avg}}} - 2\right)^{1/2} \quad (10)$$

The values of n_{D-S} are recorded in Table 3 and observed to increase with increasing the ratio of Yb^{3+} ions because of the increase in polarization within the glass matrix at high frequencies as mentioned in the next section.

Wemple–DiDomenico (WDD) model is used to calculate the static refractive index (n_o) at low frequencies, i.e., the refractive index at zero frequency ($h\nu \cong 0$). The mathematical equation that expresses WDD model is as follows [51]:

$$\left(n^2-1\right)^{-1} = \frac{E_o}{E_d} - \frac{1}{E_d E_o}(h\nu)^2, \quad (11)$$

where n is the refractive index, E_o is the single oscillator energy, E_d is the dispersion energy, and $h\nu$ is the incident photon energy. The values of E_o and E_d are determined by graphing $\left(n^2-1\right)^{-1}$ versus $(h\nu)^2$ as shown in Fig. 9. The slope of the curves equals $(-1/E_d\ E_o)$ and the intercept equals (E_o/E_d). The values of E_o and E_d are recorded in Table 4 and found to decrease as the ratio of Yb^{3+} ions increases. The observed decrease in E_d values indicates the increase in the degree of structural disorder of the glasses as the ratio of Yb^{3+} ions increase which is in line with the Urbach energy results [52]. The observed decrease in E_o values is in line with the optical bandgap results. When $h\nu$ tends to zero, Eq. (11) can be written in the next form:

$$n_o = \sqrt{1+\frac{E_d}{E_o}} \quad (12)$$

The value of n_o depends on the values of E_d and E_o. Since the decrease in the values of E_d is greater than the decrease in the values of E_o, the static refractive index decreases accordingly. The values of n_o are recorded in Table 4. The values of E_o and E_d are employed to calculate the optical spectrum moments ($M_{-1}\&M_{-3}$) and static dielectric constant (ε_∞) from the next relations [51]:

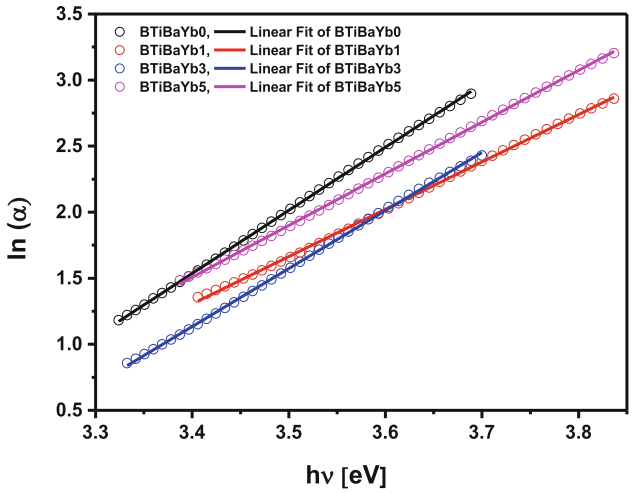

Fig. 8 ln (α) vs. $h\nu$ for Yb^{3+}-doped barium titanium borate glasses

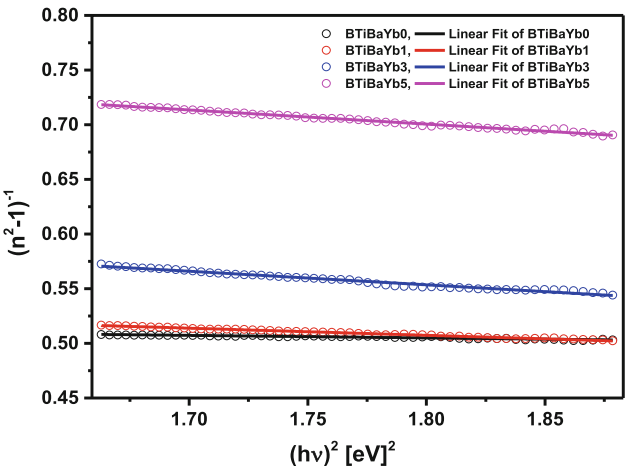

Fig. 9 $\left(n^2-1\right)^{-1}$ versus $(h\nu)^2$ for Yb^{3+}-doped barium titanium borate glasses

Table 4 Single oscillator energy (E_o), dispersion energy (E_d), static refractive index (n_o), static dielectric constant (ε_∞), and optical spectra moments (M_{-1}&M_{-3}) of Yb_2O_3 doped barium titanium borate glasses

Sample code	BTiBaYb0	BTiBaYb1	BTiBaYb3	BTiBaYb5
E_o (eV)	4.852	3.095	2.500	2.684
E_d (eV)	8.873	4.954	3.217	2.874
n_o	1.682	1.613	1.512	1.439
ε_∞	2.829	2.602	2.286	2.071
M_{-1}	1.829	1.601	1.287	1.071
$M_{-3}(\text{eV})^{-2}$	0.078	0.167	0.206	0.149

$$M_{-1} = \frac{E_d}{E_o} \& M_{-3} = \frac{E_d}{E_o^3} \tag{13}$$

$$\varepsilon_\infty = n_o^2 = 1 + \frac{E_d}{E_o} \tag{14}$$

The values of $M_{-1}, M_{-3}, \text{and} \varepsilon_\infty$ are recorded in Table 4. The values of $M_{-1}\text{and}\varepsilon_\infty$ are found to decrease with increasing the concentration of Yb^{3+} ions while the values of M_{-3} increase.

The average oscillator strength (S_o) and average oscillator wavelength (λ_o) are calculated using Sellmeier dispersion formula [53]:

$$n^2 - 1 = \frac{S_o \lambda_o^2}{1 - \left(\frac{\lambda_o^2}{\lambda^2}\right)} \tag{15}$$

Figure 10 shows the graphs of $\left(n^2-1\right)^{-1}$ versus λ^{-2} for all glasses. The slope of the curves equals $(-1/S_o)$ and the intercept equals$(1/S_o\lambda_o^2)$. The values of S_o are found to decrease with increasing the ratio of Yb^{3+} ions while the values of λ_o increase. The values of S_o and λ_o are recorded in Table 5.

The linear optical susceptibility $\chi^{(1)}$, third order non-linear optical susceptibility $\chi^{(3)}$, and non-linear refractive index n_2 are calculated from the relationships [53]:

$$\chi^{(1)} = \frac{1}{4\pi}\frac{E_d}{E_o} \tag{16}$$

$$\chi^{(3)} = 6.82 \times 10^{-15}\left(\frac{E_d}{E_o}\right)^4 (\text{esu}) \tag{17}$$

$$n_2 = 12\pi\frac{\chi^{(3)}}{n_o} \tag{18}$$

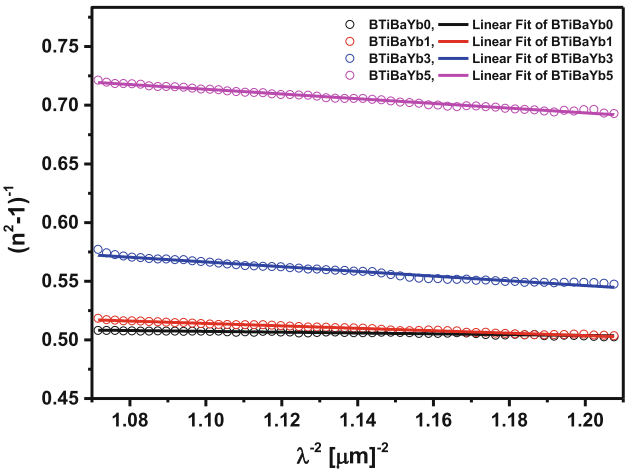

Fig. 10 $\left(n^2-1\right)^{-1}$ versus λ^{-2} for Yb^{3+}-doped barium titanium borate glasses

The values of $\chi^{(1)}$, $\chi^{(3)}$, and n_2 are recorded in Table 5 and found to decrease with increasing the concentration of Yb^{3+} ions due to the great decrease in the values of E_d compared to that of E_o. Figure 11 shows the variations of linear, static, and non-linear refractive indices as a function of Yb_2O_3 content. The observed linear behavior of n_{D-S} in Fig. 11 is represented by an empirical equation as follows:

$$n_{D-S} = 0.01603x_{Yb_2O_3} + 2.34752 \tag{19}$$

where x_{Yb2O3} is the molar fraction of Yb_2O_3. The linear refractive index of the studied glasses strongly depends on the concentration of Yb^{3+} ions. Figure 12 shows the variations of third order non-linear optical susceptibility and static dielectric constant as a function of of Yb_2O_3 content.

3.8 Metallization criterion and optical basicity

Lorentz–Lorentz equation correlates the molar refraction (R_m) of the studied glasses with the linear refractive index (n_{D-S}) and molar volume (V_m) as follows [54]:

$$R_m = \left(\frac{n_{D-S}^2 - 1}{n_{D-S}^2 + 2}\right)V_m \tag{20}$$

The molar electronic polarizability (α_m) is proportional to the molar refraction (R_m) and given by:

$$\alpha_m = \left(\frac{3}{4\pi N_A}\right)R_m \tag{21}$$

Table 5 Average oscillator strength (S_o), average oscillator wavelength (λ_o), linear optical susceptibility ($\chi^{(1)}$), third order non-linear optical susceptibility ($\chi^{(3)}$), and non-linear refractive index

Sample code	BTiBaYb0	BTiBaYb1	BTiBaYb3	BTiBaYb5
$S_o \times 10^{-6}$ (nm)$^{-2}$	28.353	9.667	4.970	4.965
λ_o (nm)	254.144	405.926	505.398	464.077
$\chi^{(1)}$	0.146	0.127	0.102	0.085
$\chi^{(3)} \times 10^{-14}$ (esu)	7.628	4.477	1.870	0.897
$n_2 \times 10^{-13}$	17.097	10.464	4.663	2.350

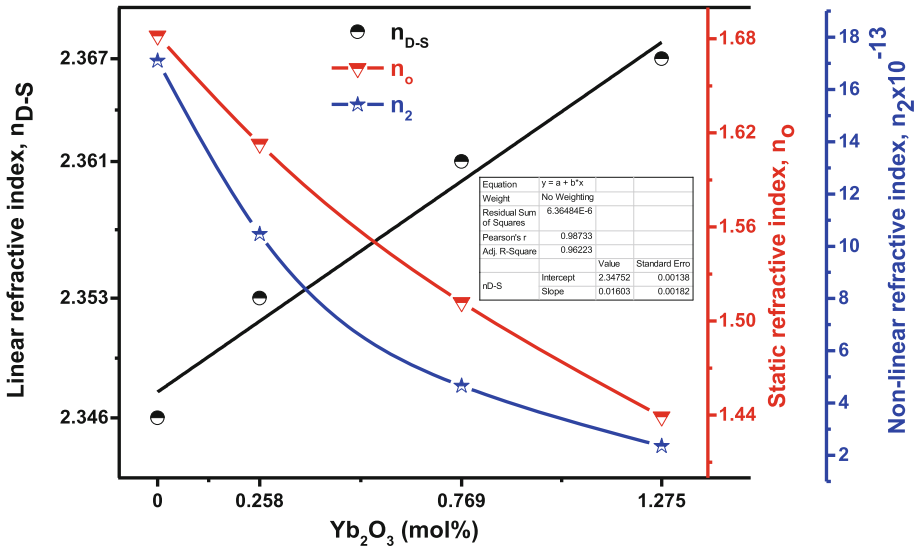

Fig. 11 Linear, static, and non-linear refractive indices as a function of Yb_2O_3 content

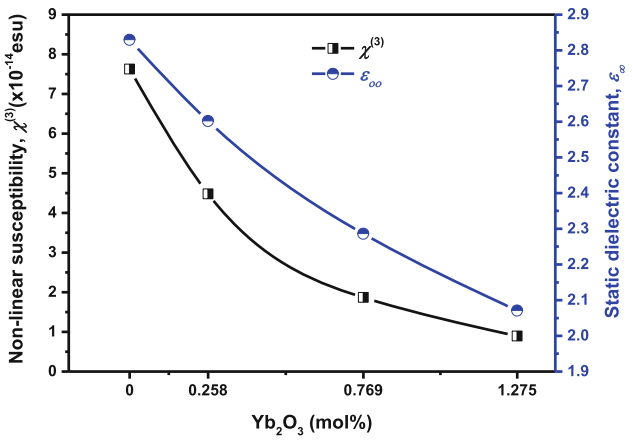

Fig. 12 Third order non-linear optical susceptibility and static dielectric constant as a function of of Yb_2O_3 content

The values of R_m and α_m are calculated and listed in Table 6. As seen from Table 6, the R_m and α_m tend to increase with increasing the ratio of Yb^{3+} ions. The metallization criterion (M_C) is utilized to obtain information about the non-metallic behavior of solids based on the relation [45]:

$$M_C = 1 - \frac{R_m}{V_m} \tag{22}$$

when the value of M_C approaches one, the material is classified as an insulator while when the value of M_C approaches zero, the material classified as a metal. The values of M_C of the studied glasses are calculated and found to decrease from 0.400 to 0.394 with increasing the concentration of Yb^{3+} ions. The values of M_C (0.394–0.400) lie in between insulators and metals, i.e., the studied glasses behave as semiconductors. The dependance of the molar electronic polarizability and metallization criterion on the Yb_2O_3 content is presented in Fig. 13.

The oxide ion polarizability $\alpha_{O^{2-}}(n_{D-S})$ and optical basicity $\Lambda(n_{D-S})$ of the studied glasses can be calculated based on the linear refractive index using the next relations [55]:

$$\alpha_{O^{2-}}(n_{D-S}) = \left[\frac{R_m}{2.52} - \sum \alpha_{cat}\right](N_{O^{2-}})^{-1} \tag{23}$$

$$\Lambda(n_{D-S}) = 1.67\left(1 - \frac{1}{\alpha_{O^{2-}}}\right), \tag{24}$$

Table 6 Molar refraction R_m, molar electronic polarizability α_m, metallization criterion M_C, oxide ion polarizability $\alpha_{O^{2-}}$, and optical basicity Λ of Yb_2O_3-doped barium titanium borate glasses

Sample code	R_m (cm^3/mol)	α_m ($Å^3$)	M_C	$\alpha_{O^{2-}}$ ($Å^3$)	Λ
BTiBaYb0	16.731	6.639	0.400	2.7787	1.0690
BTiBaYb1	16.729	6.638	0.398	2.7742	1.0680
BTiBaYb3	16.779	6.658	0.396	2.7753	1.0683
BTiBaYb5	16.988	6.741	0.394	2.8055	1.0747

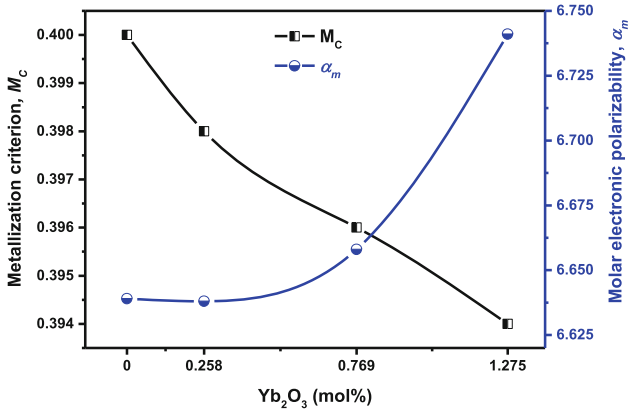

Fig. 13 Molar electronic polarizability and metallization criterion as a function of Yb_2O_3 content

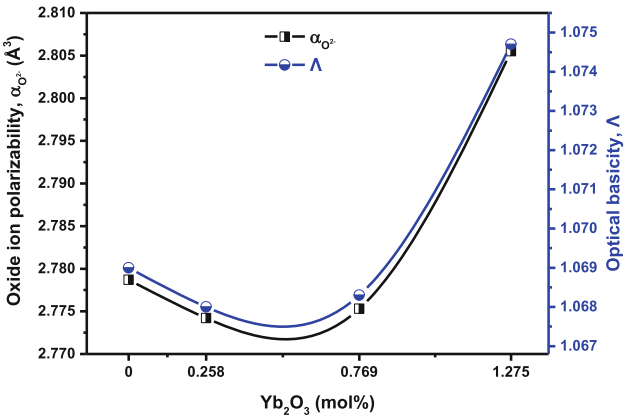

Fig. 14 Oxide ion polarizability and optical basicity as a function of Yb_2O_3 content

where $\sum \alpha_{cat}$ is the molar cation polarizability and $N_{O^{2-}}$ is the number of oxide ions in the chemical formula of the glass composition. The dependance of the $\alpha_{O^{2-}}(n_{D-S})$ and $\Lambda(n_{D-S})$ on Yb_2O_3 content is presented in Fig. 14. As seen from Fig. 14, the $\alpha_{O^{2-}}(n_{D-S})$ and $\Lambda(n_{D-S})$ tend to increase as the ratio of Yb^{3+} ions increases due to the increase in the molar refraction (R_m). The values of $\alpha_{O^{2-}}(n_{D-S})$ and $\Lambda(n_{D-S})$ are listed in Table 6.

3.9 Absorption–emission cross sections and gain spectra

The absorption $\sigma_{abs}(\lambda)$ and emission $\sigma_{emis}(\lambda)$ cross-sections for $^2F_{5/2} \rightarrow {}^2F_{7/2}$ transition of Yb^{3+} ions are calculated based on the the optical absorbance (A), Yb^{3+} ions concentration (N), and glass thickness (L) by the next relationships [56]:

$$\sigma_{abs}(\lambda) = 2.303A(\lambda)/NL \tag{25}$$

$$\sigma_{emis}(\lambda) = \sigma_{abs}(\lambda)\frac{Z_l}{Z_u}\exp\left[\left(E_{zl} - \frac{hc}{\lambda}\right)/K_B T\right], \tag{26}$$

where Z_l and Z_u are the partitioning functions of the lower and upper states, respectively, E_{Zl} is the energy difference between the ground state and upper state manifold, and T is the room temperature. The obtained values of the absorption and emission cross-sections for $^2F_{5/2} \rightarrow {}^2F_{7/2}$ transition are displayed in Fig. 15. The peaks of the emission cross-section (σ_{emis}) have the values of 16.284×10^{-21}, 20.062×10^{-21}, and 16.315×10^{-21} cm^{-2} for BTiBaYb1, BTiBaYb3, and BTiBaYb5 glasses, respectively. The high values of σ_{emis} make the present glasses strong candidate for laser and amplifier applications. Moreover, the wide emission is helpful for the creation of tunable and ultra-short pulse lasers [57].

The optical gain coefficient $G(\lambda)$ can be calculated based on the values of the absorption and emission cross-sections using the next relation [56]:

$$G(\lambda) = \sigma_{emis}(\lambda)NP - \sigma_{abs}(\lambda)N(1-P), \tag{27}$$

where P is the rate of population inversion of $^2F_{5/2} \rightarrow {}^2F_{7/2}$ transition and taken as: 0, 0.1, 0.2, 0.3, 0.4, 0.5, 0.6, 0.7, 0.8, 0.9, and 1.0. The obtained values of $G(\lambda)$ are displayed in Fig. 16, and it is noted that the gain coefficient and gain band increase as the value of P increases, and the gain will be completely flat when the value of P is greater than 0.6. Furthermore, the gain spectra exhibit positive values in the wavelength range 971–1010 nm when the values of P are greater than 0.3.

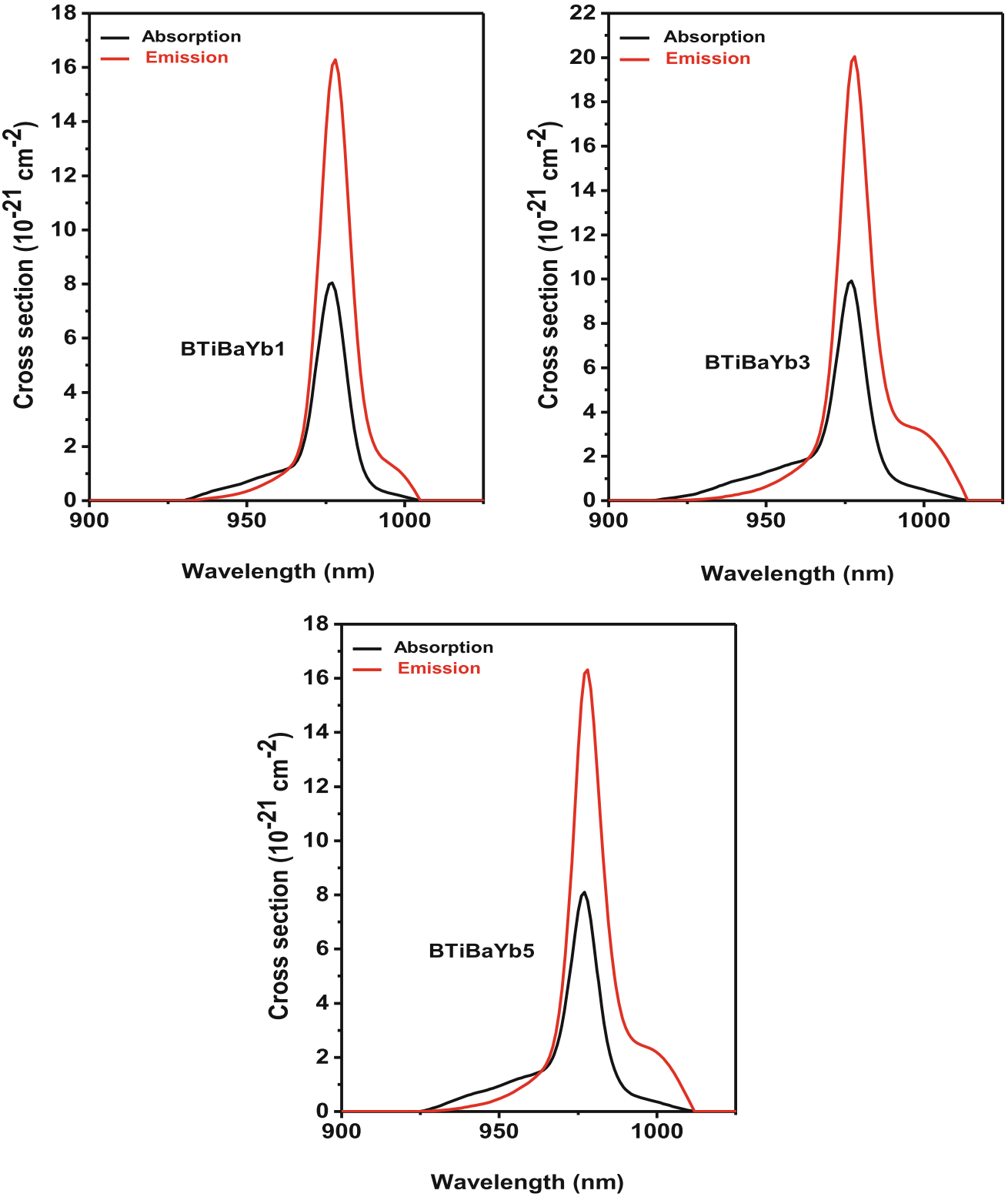

Fig. 15 Absorption and emission cross-sections for $^2F_{5/2} \rightarrow {}^2F_{7/2}$ transition of Yb^{3+}-doped barium titanium borate glasses

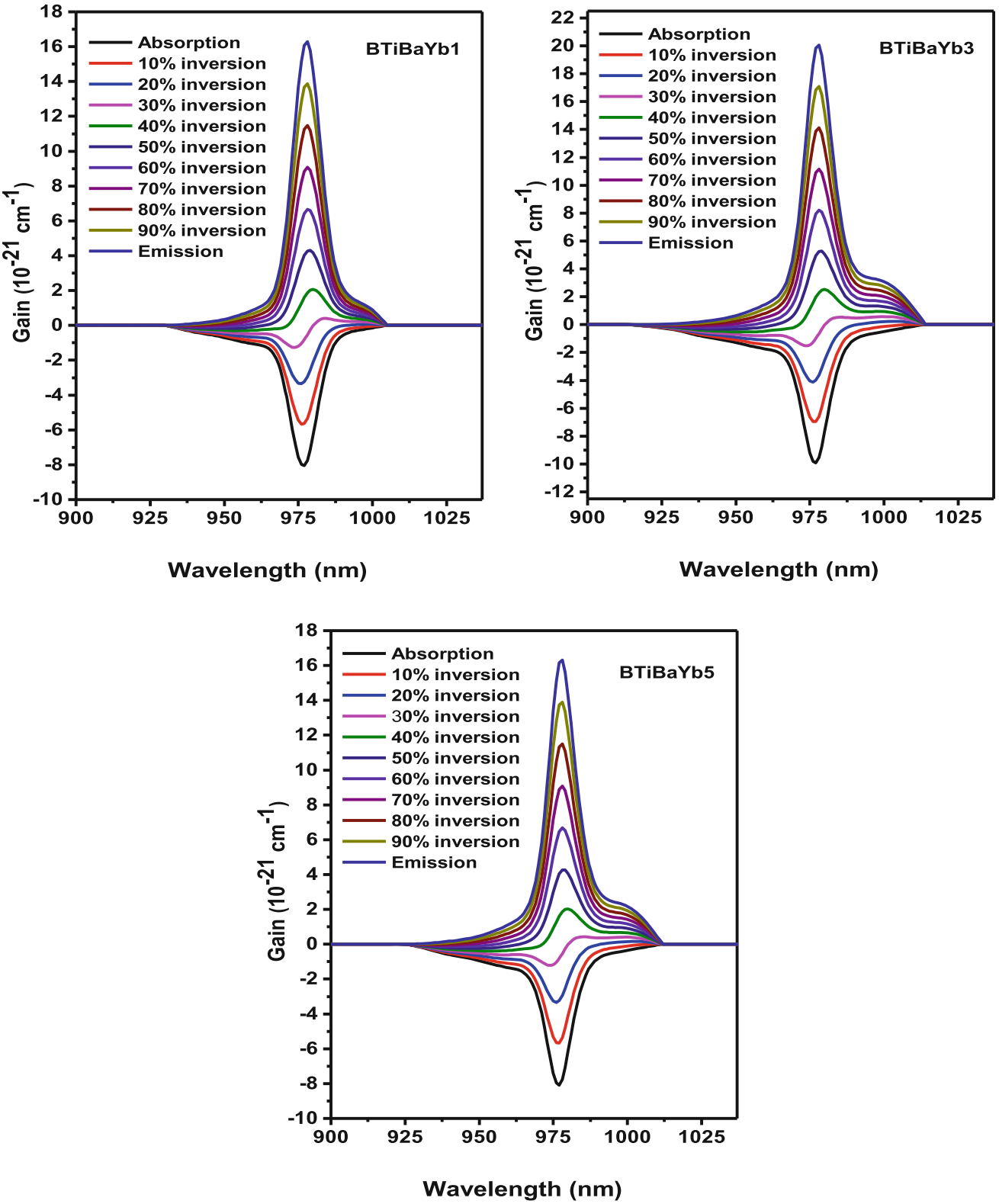

Fig. 16 Gain coefficient for $^2F_{5/2} \rightarrow {}^2F_{7/2}$ transition of Yb^{3+}-doped barium titanium borate glasses

4 Conclusion

The density of the studied glasses increased with increasing the concentration of Yb_2O_3 from 3.652 to 3.761 g/cm^3 while the molar volume decreased from 27.875 to 27.784 cm^3/mol then increased to 28.06 cm^3/mol. The distinctive bands of FTIR and Raman spectra were described and identified. The optical bandgap and metallization criterion decreased with increasing the ratio of Yb_2O_3 while the linear refractive index increased. The average oscillator strength, linear and non-linear optical susceptibilities, and non-linear refractive index decreased with increasing the ratio of Yb_2O_3. The absorption and emission cross-sections and gain coefficients for $^2F_{5/2} \rightarrow {}^2F_{7/2}$ transition of Yb^{3+} ions were calculated. The high values of emission cross-sections of the studied glasses made them strong candidates for laser and amplifier applications. Furthermore, the wide emission is helpful for creating tunable and ultra-short pulse lasers.

Author contributions

SYM: Conceptualization, Methodology, Writing—review and editing. MAA: Conceptualization, Formal analysis, Writing—review and editing. HME: Formal analysis, Software, Writing—original draft. NAZ: Supervision, Methodology. WA: Supervision, Instruments, Methodology.

Funding

Open access funding provided by The Science, Technology & Innovation Funding Authority (STDF) in cooperation with The Egyptian Knowledge Bank (EKB). The authors declare that no funds, grants, or other support were received during the preparation of this manuscript.

Data availability

The datasets generated during the current study are available from the corresponding author on reasonable request.

Research data policy

The datasets are presented in the main manuscript.

Declarations

Conflict of interests The authors declare that they have no known competing financial interests or personal relationships that could have appeared to influence the work reported in this paper.

References

1. R.A. Talewar, S. Mahamuda, K. Swapna, M. Venkateswarlu, A.S. Rao, Spectroscopic studies of Sm^{3+} ions doped alkaline-earth chloro borate glasses for visible photonic applications. Mater. Res. Bull. **105**, 45–54 (2018)
2. L. Shamshad, G. Rooh, K. Kirdsiri, N. Srisittipokakun, B. Damdee, H.J. Kim, J. Kaewkhao, Effect of alkaline earth oxides on the physical and spectroscopic properties of Dy^{3+}-doped Li_2O-B_2O_3 glasses for white emitting material application. Opt. Mater. **64**, 268–275 (2017)
3. S. Yusub, C. Rajyasree, A.R. Babu, P.M.V. Teja, D.K. Rao, Influence of alkaline earth oxides (R = Ca, Sr and Ba) on spectroscopic and dielectric studies of iron doped RO–Na_2O–B_2O_3 glasses. J. Non-Cryst. Solids **364**, 62–68 (2013)
4. A.L. Martins Jr., C.A.C. Feitosa, W.Q. Santos, C. Jacinto, C.C. Santos, Influence of BaX_2 (X = Cl, F) and Er_2O_3 concentration on the physical and optical properties of barium borate glasses. Physica B **558**, 146–153 (2019)

5. H. Othman, H. Elkholy, M.R. Cicconi, D. Palles, D. de Ligny, E.I. Kamitsos, D. Möncke, Spectroscopic study of the role of alkaline earth oxides in mixed borate glasses-site basicity, polarizability and glass structure. J. Non-Cryst. Solids **533**, 119892 (2020)
6. S.R. Narisimsetti, M. Rajesh, G.R. Reddy, B.D.P. Raju, S. Danapandian, Study of influence of Sm^{3+} ions concentration on fluorescence and FT-IR studies of lead barium lithium borate glasses for red color display device applications. Opt. Mater. **97**, 109360 (2019)
7. S.B. Kolavekar, N.H. Ayachit, Impact of Pr_2O_3 on the physical and optical properties of multi-component borate glasses. Mater. Chem. Phys. **257**, 123796 (2021)
8. K. Sathish, S. Thirumaran, Spectroscopic and ultrasonic investigations on structural characterization of borate glass specimen doped with transition metal ions. Spectrochim. Acta A **147**, 163–172 (2015)
9. A. Bhogi, R.V. Kumar, P. Kistaiah, Effect of alkaline earths on spectroscopic and structural properties of Cu^{2+} ions-doped lithium borate glasses. J. Non-Cryst. Solids **426**, 47–54 (2015)
10. S. Selvi, K. Marimuthu, G. Muralidharan, Effect of PbO on the B_2O_3–TeO_2–P_2O_5–BaO–CdO–Sm_2O_3 glasses-structural and optical investigations. J. Non-Cryst. Solids **461**, 35–46 (2017)
11. F.A. Moustafa, A.M. Fayad, F.M. Ezz-Eldin, I. El-Kashif, Effect of gamma radiation on ultraviolet, visible and infrared studies of NiO, Cr_2O_3 and Fe_2O_3-doped alkali borate glasses. J. Non-Cryst. Solids **376**, 18–25 (2013)
12. H.A. El Batal, E.M. Abou Hussein, N.A. El Alaily, F.M. Ezz Eldin, Effect of different 3d transition metal oxides on some physical properties of γ-irradiated Bi_2O_3–B_2O_3 glasses: a comparative study. J. Non-Cryst. Solids **528**, 119733 (2020)
13. N.R. Lakshmi, S. Cole, Influence of TiO_2 ions on spectroscopic properties of oxyfluoride glasses. Mater. Today **18**, 192–206 (2019)
14. N.A. El-Alaily, E.M. Abou Hussein, F.M. Ezz Eldin, Gamma irradiation and heat treatment effects on barium borosilicate glasses doped titanium oxide. J. Inorg. Organomet. Polym. Mater. **28**, 2662–2676 (2018)
15. L. Singh, V. Thakur, R. Punia, R.S. Kundu, A. Singh, Structural and optical properties of barium titanate modified bismuth borate glasses. Solid State Sci. **37**, 64–71 (2014)
16. Y.B. Saddeek, H.M. Zakaly, K.C. Sekhar, S.A. Issa, T. Alharbi, A. Badawi, M. Shareefuddin, Investigations of mechanical and radiation shielding properties of $BaTiO_3$-modified cadmium alkali borate glass. Appl. Phys. A **128**, 1–10 (2022)
17. S.K. Lenkennavar, M.K. Kokila, B. Eraiah, Spectroscopic investigation of different nano metals doped to lead sodium calcium borate glasses. Mater. Today **26**, 1167–1174 (2020)
18. L.M. Marcondes, L. Rodrigues, C.R. da Cunha, R.R. Gonçalves, A.S.S. de Camargo, F.C. Cassanjes, G.Y. Poirier, Rare-earth ion doped niobium germanate glasses and glass-ceramics for optical device applications. J. Lumin. **213**, 224–234 (2019)
19. K.V. Rao, S. Babu, C. Balanarayana, Y.C. Ratnakaram, Comparative impact of Nd^{3+} ion doping concentration on near-infrared laser emission in lead borate glassy materials. Optik **202**, 163562 (2020)
20. A. Ibrahim, M.A. Farag, M.S. Sadeq, Towards highly transparent tungsten zinc sodium borate glasses for radiation shielding purposes. Ceram. Int. **48**, 12079–12090 (2022)
21. M.A. Algradee, E.E. Saleh, T.M.E.L. Sherbini, R. El-Mallawany, Optical and gamma-ray shielding features of Nd^{3+} doped lithium-zinc-borophosphate glasses. Optik **242**, 167059 (2021)
22. K.S. Shaaban, A.M. Al-Baradi, E.A. Wahab, The impact of Y_2O_3 on physical and optical characteristics, polarizability, optical basicity, and dispersion parameters of B_2O_3–SiO_2–Bi_2O_3–TiO_2 glasses. Silicon **14**, 5057–5065 (2022)
23. M.S. Gaafar, S.Y. Marzouk, I.S. Mahmoud, Role of dysprosium on some acoustic and physical properties of PbO–B_2O_3–SiO_2 glasses. Results Phys. **22**, 103944 (2021)
24. V. Aruna, S. Yusub, M. Venkateswarlu, A.R. Babu, K. Anitha, Efficacy of copper ions on lithium ion conductivity, electron hopping, optical band gap, metallization criterion and morphology of Li_2O–B_2O_3–P_2O_5 glasses. J. Non-Cryst. Solids **536**, 120015 (2020)
25. P. Kaur, K.J. Singh, S. Thakur, P. Singh, B.S. Bajwa, Investigation of bismuth borate glass system modified with barium for structural and gamma-ray shielding properties. Spectrochim. Acta A **206**, 367–377 (2019)
26. N. Gupta, A. Kaur, A. Khanna, F. Gonzàlez, C. Pesquera, R. Iordanova, B. Chen, Structure-property correlations in TiO_2–Bi_2O_3–B_2O_3–TeO_2 glasses. J. Non-Cryst. Solids **470**, 168–177 (2017)
27. A.S. Abu-Khadra, A.M. Taha, A.M. Abdel-Ghany, A.A. Abul-Magd, Effect of silver iodide (AgI) on structural and optical properties of cobalt doped lead–borate glasses. Ceram. Int. **47**, 26271–26279 (2021)
28. A. Dehelean, S. Rada, J. Zhang, Determination of the lead environment in samarium–lead oxide-borate glasses and vitroceramics using XANES and EXAFS studies. Radiat. Phys. Chem. **174**, 108927 (2020)
29. L. Vijayalakshmi, K.N. Kumar, C. Tirupataiah, J.D. Baek, P. Hwang, Biocompatible and UV triggered energy transfer based color tunable emission from Ce^{3+}/Eu^{3+} co-doped

lithium zinc borate glasses for white light applications. J. Non-Cryst. Solids **577**, 121312 (2022)
30. M. Djamal, L. Yuliantini, R. Hidayat, N. Rauf, M. Horprathum, R. Rajaramakrishna, K. Boonin, P. Yasaka, J. Kaewkhao, V. Venkatramu, Spectroscopic study of Nd^{3+} ion-doped Zn–Al–Ba borate glasses for NIR emitting device applications. Opt. Mater. **107**, 110018 (2020)
31. T.D.P.V. Jalluri, K.V. Sriram, B. Rudraswamy, V. Hegde, G. Devarajulu, K.N.N. Prasad, A.G. Pramod, D.A. Aloraini, A.H. Almuqrin, M.I. Sayyed, Photoluminescence and nonlinear optical investigations on Eu_2O_3 doped sodium bismuth borate glasses for solid state lighting and near-infrared optical limiting applications. Infrared Phys. Technol. **116**, 103784 (2021)
32. M.M. Neethish, J.N. Acharyya, G.V. Prakash, V.V.R.K. Kumar, Effect of zinc fluoride addition on structure of barium borate glasses for nonlinear optical applications. Opt. Mater. **121**, 111626 (2021)
33. G. Jagannath, M.I. Sayyed, A.M.S. Alhuthali, Nanosecond nonlinear optical, optical limiting and gamma radiation shielding attributes of Eu^{3+} ions doped heavy metal borate glasses. Ceram. Int. **47**, 14330–14340 (2021)
34. P. Kaur, K.J. Singh, S. Thakur, M. Kurudirek, M.M. Rafiei, Structural investigations and nuclear radiation shielding ability of bismuth lithium antimony borate glasses. J. Phys. Chem. Solids **150**, 109812 (2021)
35. M.R. Ahmed, B. Ashok, S.K. Ahmmad, A. Hameed, M.N. Chary, M. Shareefuddin, Infrared and Raman spectroscopic studies of Mn^{2+} ions doped in strontium alumino borate glasses: describes the role of Al_2O_3. Spectrochim. Acta A **210**, 308–314 (2019)
36. K.C. Sekhar, M. Shareefuddin, A. El-Denglawey, Y.B. Saddeek, Structural and optical properties of $BaTiO_3$ modified cadmium alkali borate glasses. Phys. Scr. **97**, 035704 (2022)
37. M.A. Marzouk, F.H. ElBatal, H.A. ElBatal, Effect of TiO_2 on the optical, structural and crystallization behavior of barium borate glasses. Opt. Mater. **57**, 14–22 (2016)
38. E.K. Abdel-Khalek, E.A. Mohamed, S.M. Salem, F.M. Ebrahim, I. Kashif, Study of glass-nanocomposite and glass-ceramic containing ferroelectric phase. Mater. Chem. Phys. **133**, 69–77 (2012)
39. H.A. ElBatal, A.M. Abdelghany, N.A. Ghoneim, F.H. ElBatal, Effect of 3d-transition metal doping on the shielding behavior of barium borate glasses: a spectroscopic study. Spectrochim. Acta A **133**, 534–541 (2014)
40. P.K. Pothuganti, A. Bhogi, M.R. Kalimi, P.S. Reniguntla, Influence of TiO_2 ions on structural properties and AC conductivity of $BaO–Bi_2O_3–B_2O_3$ glass system. Mater. Today **38**, 2200–2204 (2021)
41. F.H. ElBatal, M.A. Marzouk, H.A. ElBatal, Crystallization and spectroscopic characterizations of binary $SrO–B_2O_3$ glasses doped with LiF, NaF, CaF_2, or TiO_2. J. Aust. Ceram. Soc. **55**, 1039–1049 (2019)
42. S.Y. Marzouk, M.A. Azooz, H.A. El Batal, Judd-Ofelt analysis of spectroscopic measurements of Er^{3+} doped boro-zincate glasses. J. Mol. Struct. **1243**, 130925 (2021)
43. G. Kilic, E. Ilik, S.A.M. Issa, B. Issa, M.S. Al-Buriahi, U.G. Issever, H.M.H. Zakaly, H.O. Tekin, Ytterbium(III) oxide reinforced novel $TeO_2–B_2O_3–V_2O_5$ glass system: synthesis and optical, structural, physical and thermal properties. Ceram. Int. **47**, 18517–18531 (2021)
44. A. Edukondalu, B. Kavitha, M.A. Samee, S.K. Ahmmed, S. Rahman, K.S. Kumar, Mixed alkali tungsten borate glasses–optical and structural properties. J. Alloys Compd. **552**, 157–165 (2013)
45. S.Y. Marzouk, A.H. Hammad, H.M. Elsaghier, W. Abbas, N.A. Zidan, The correlation between the structural, optical, and electrical properties in mixed alkali fluoroborate glasses containing vanadium ions. J. Non-Cryst. Solids **476**, 30–35 (2017)
46. A.H. Hammad, H.M. Elsaghier, W. Abbas, N.A. Zidan, S.Y. Marzouk, Investigation of some structural and optical properties of lithium sodium fluoroborate glasses containing cuprous oxide. Measurement **116**, 170–177 (2018)
47. A.S. Abouhaswa, R. El-Mallawany, Y.S. Rammah, Direct influence of La on structure, optical and gamma-ray shielding properties of lead borate glasses. Radiat. Phys. Chem. **177**, 109085 (2020)
48. Ö.B. Mergen, E. Arda, Determination of optical band gap energies of CS/MWCNT bio-nanocomposites by Tauc and ASF methods. Synth. Met. **269**, 116539 (2020)
49. O.I. Sallam, A. Abdel-Galil, N.L. Moussa, Optimizing of optical and structure characters of borate glasses by different concentration of CoO: electron beam irradiation dosimetry. Mater. Chem. Phys. **269**, 124767 (2021)
50. A.A. El-Daly, M.A. Abdo, H.A. Bakr, M.S. Sadeq, Structure, stability and optical parameters of cobalt zinc borate glasses. Ceram. Int. **47**, 31470–31475 (2021)
51. A.M.A. Shamekh, A.Z. Mahmoud, M.A. Abdel-Rahim, Assessment of linear/nonlinear optical constants and dispersion parameters of $Se_{85-x}Te_{15}Sb_x$ glasses for photonic applications. Opt. Mater. **114**, 111008 (2021)
52. D.J. Borah, A.T.T. Mostako, Investigation on dispersion parameters of molybdenum oxide thin films via Wemple–DiDomenico (WDD) single oscillator model. Appl. Phys. A **126**, 1–13 (2020)
53. A.M. Alsaad, Q.M. Al-Bataineh, A.A. Ahmad, Z. Albataineh, A. Telfah, Optical band gap and refractive index dispersion parameters of boron-doped ZnO thin films: a novel derived

mathematical model from the experimental transmission spectra. Optik **211**, 164641 (2020)
54. S.A. Umar, M.K. Halimah, G.G. Ibrahim, I.O. Alade, M.N. Azlan, R. El-Mallawany, A.M. Hamza, S.N. Nazrin, L.U. Grema, M.S. Otto, Oxide ion/electronic polarizability, optical basicity and linear dielectric susceptibility of TeO_2–B_2O_3–SiO_2 glasses. Ceram. Int. **47**, 21668–21678 (2021)
55. X. Zhao, X. Wang, H. Lin, Z. Wang, Correlation among electronic polarizability, optical basicity and interaction parameter of Bi_2O_3–B_2O_3 glasses. Physica B **390**, 293–300 (2007)
56. H.M. Elsaghier, M.A. Azooz, N.A. Zidan, W. Abbas, A. Okasha, S.Y. Marzouk, Spectroscopic and optical investigations on Er^{3+} ions doped alkali cadmium phosphate glasses for laser applications. J. Non-Cryst. Solids **588**, 121616 (2022)
57. K.V. Krishnaiah, K.U. Kumar, V. Agarwal, C.G. Murali, S. Chaurasia, L.J. Dhareshwar, C.K. Jayasankar, V. Lavin, Fluorescence and spectroscopic properties of Yb^{3+}-doped phosphate glasses. Phys. Procedia **29**, 109–113 (2012)